RSC Advances

PAPER

View Article Online
View Journal | View Issue

Cite this: *RSC Adv.*, 2021, **11**, 31124

Zinc porphyrin/mesoporous titania thin film electrodes: a hybrid material nanoarchitecture for photocatalytic reduction†

Rolando M. Caraballo, Priscila Vensaus, Facundo C. Herrera, Galo J. A. A. Soler Illia and Mariana Hamer *

Received 1st September 2021
Accepted 10th September 2021

DOI: 10.1039/d1ra06585h

rsc.li/rsc-advances

In this work, photocatalytic reduction of methyl viologen is achieved using zinc tetra(4-*N*-methylpyridyl) porphine (ZnP) functionalized mesoporous titania thin films (MTTF). Metalloporphyrins are the core of natural systems that harvest energy from the sun. Thus, a bioinspired approach is used, taking advantage of ZnP sensitizing capabilities and MTTF organized structure.

Introduction

Global warming has accelerated over the last decades. The cause for this phenomenon is anthropogenic and how to cope with it has become one of humanity's biggest challenges.[1,2] To do so, an economy based on renewable energy sources has become essential, with solar energy as one of the most attractive alternatives.

In nature, photosynthesis is the most efficient method to capture and store solar energy. To achieve this, photosynthetic organisms have complex organized structures that include tetrapyrrolic systems.[3,4] These molecules have high molar absorptivity in the visible portion of the spectra, where the solar photon flux has its maximum, leading to an efficient harvest of sunlight. Porphyrins and metalloporphyrins (MP) also act as catalysts at the reaction center in natural enzymes because, due to planar coordination rigidity, two *trans* axial positions remain free for substrate coordination. Therefore, mimicking their behavior in biological systems, MP are used to design sustainable energy solutions,[5] where they can act both as antennas and reaction centers. Following this approach, MP have become the cornerstone in systems for solar energy harvest like photoelectrochemical (PEC) devices[6] and dye-sensitized solar cells (DSSC).[7–9] But, even if the source is renewable, energy needs to be stored and delivered without damaging the environment.[10] Thus, the synthesis of clean fuels is a milestone for sustainability, with water splitting as a top candidate, given the abundance of raw material and the high energy density of H_2.[11,12] MP were first used in oxidation reactions,[13,14] but they can also catalyze reactions such as hydrogen generation or CO_2 reduction,[15] becoming an attractive alternative as catalyzers for the production of clean fuels.[16,17] Among all MP, the ones containing zinc are the most studied in photochemical systems because of their relatively high thermal stability, robustness under light exposure, straightforward synthesis, low toxicity and photophysical properties. They also have lower oxidation potentials than their free base analogues, which results in a more efficient electron injection and dye regeneration.[18]

To achieve the spatial organization observed in nature and generate new properties, porphyrin's structure can be modified to tune their physicochemical properties.[19] This allows them to act as molecular building blocks in the development of multifunctional materials with different levels of organization.[5,20,21] These structures can be obtained through self-assembly or using a scaffold, such as TiO_2, ZrO_2, CeO_2 and other inorganic semiconductors with robust architectures.[22,23] The combination of porphyrins and MP with these semiconductors produces hybrid materials with synergetic properties and a broad range of applications.[24] TiO_2 based materials are some of the more explored scaffolds. Its combination with MP have been used in photocatalytic oxidation reactions, enhancing titania capabilities for this purpose,[25,26] together with reduction reactions of small molecules[27] and as sensitizer in DSSC, where a 13% efficiency was reached.[28] Furthermore, TiO_2 architectures can be obtained through soft, readily scalable soft methods that enable its use on applications at a bigger scale.[29]

In recent years, Soler Illia's research group comprehensively described the preparation of MTTF with an accessible, organized pore network that are transparent in the visible range.[30,31] MTTF are interesting scaffold materials, but they only absorb UV light, which corresponds roughly to 4% of the total solar spectrum. This is why dye-sensitization is used to broaden the absorption range, take advantage of the full spectrum and increase its efficiency as a solar cell.[32] In our most recent publication we have proved the inclusion of cationic MP inside an MTTF-based photonic crystal to develop an optical sensor.[23]

Instituto de Nanosistemas, Universidad Nacional de General San Martín-CONICET, Av. 25 de Mayo 1021 (B1650KNA), San Martín, Argentina. E-mail: mhamer@unsam.edu.ar

† Electronic supplementary information (ESI) available. See DOI: 10.1039/d1ra06585h

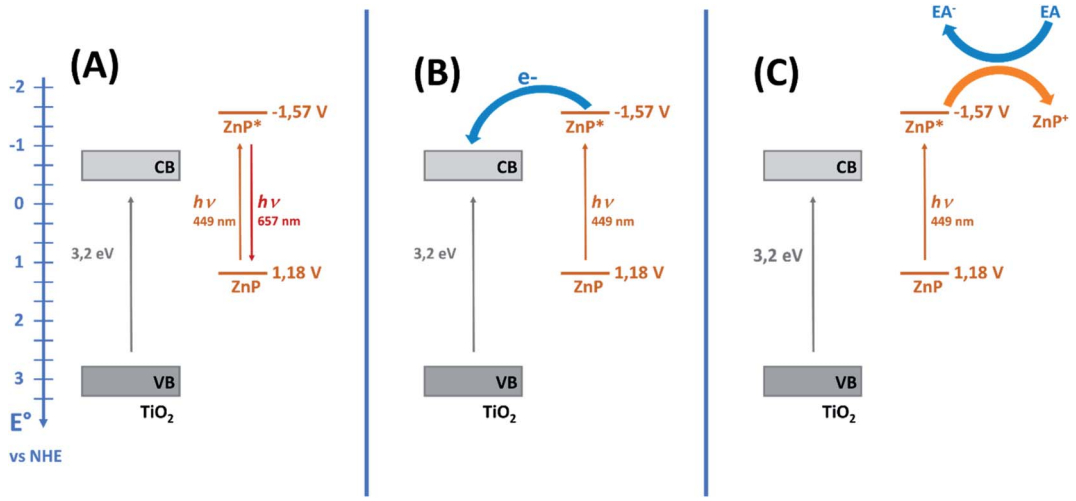

Fig. 1 Excited-state decay paths for TiO_2 surface-attached ZnP, light emission (A), charge injection (B) and reduction of an electron acceptor EA (C).

Therefore, MP can also be used to sensitize and perform reactions within the pores. In this approach, MP absorbs photons with energy smaller than the band-gap of the semiconductor. Once a photon is absorbed, the dye in its excited state can follow three pathways: (i) decay radiatively or non-radiatively (Fig. 1A); (ii) inject electrons in the conduction band of the semiconductor, which travel towards the external circuit and end up in the counter electrode (Fig. 1B); (iii) or reduce an external electron acceptor (Fig. 1C). If the electron transfer occurs, the dye is reestablished by a reducing agent.

In this work, we report the preparation of a hybrid material using ZnP for MTTF functionalization, after which its pore network remains accessible. The obtained ZnP@MTTF shows active photocatalytic performance for methyl viologen reduction, an electron relay suitable for hydrogen generation. It also retains ZnP emission properties and presents dye sensitizing capabilities. The combination of the MTTF nanoarchitecture with the photochemical properties of ZnP makes the resulting material a versatile platform for photocatalytic devices design.

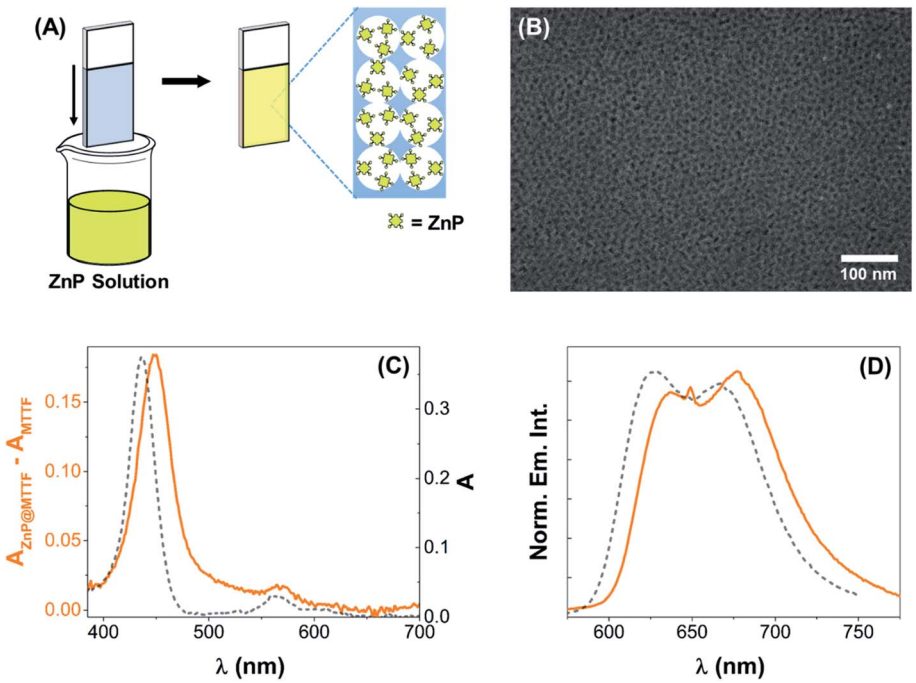

Fig. 2 Schematic representation of ZnP@MTTF synthesis (A) and FE-SEM image showing its pore structure (B). UV-Vis absorption spectra of ZnP in solution (black, dashed line) and ZnP@MTTF (orange, solid line). (C) Normalized emission spectra of ZnP in solution (black, dashed line) and ZnP@MTTF (orange, solid line) (D).

Results and discussions

Synthesis of ZnP@MTTF, schematized in Fig. 2A, is performed through immersion of an MTTF film in a ZnP solution, followed by rinsing and air-drying. Fig. 2B shows a high-resolution FE-SEM image of ZnP@MTTF where the ordered pore array characteristic of an MTTF architecture can be seen.[30,33–35] These images show no evidence of pore clogging or residues generated outside the pores. Furthermore, XRR measurements (Fig. S1A†) show a change in accessible porosity from 34% for MTTF to 29% for vacuum-dried ZnP@MTTF, indicating that ZnP gets inside the pores without occluding them, binding to the walls. To further disregard changes on the film external surface a contact angle test was performed (Fig. S2 and Table S1†), showing ZnP@MTTF and MTTF behave the same way, and wettability properties are retained.[36]

After functionalization, the film acquires a yellow coloration perceived through the naked eye (Fig. S3†). UV-Vis absorption spectrum of ZnP@MTTF with an MTTF blank, presented in Fig. 2C, shows the electronic transitions characteristic of MP, corresponding to the Soret and two *Q* absorption bands ($\lambda_{ZnP@MTTF} = 449$ nm, 568 nm and *ca.* 615 nm, respectively). All bands are red shifted compared to ZnP in solution ($\lambda_{ZnP} =$ 436 nm, 563 nm and 609 nm),[18] but the change is larger for the Soret band. This is due to the interaction of the positively charged porphyrin with the surface.[37] It is noteworthy that no new absorption bands are observed, reflecting that ZnP does not self-assemble or aggregate on the surface.[22,38,39] Likewise, ZnP emission properties in solution are retained after its attachment to the surface, with a change in emission intensity ratio of the bands (Fig. 2D). ZnP@MTTF emits in the visible range when excited in the Soret band (Fig. S4,† $\lambda_{Ex} = 449$ nm, $\lambda_{Em} = 637$ and 677 nm), red shifted compared to ZnP in solution ($\lambda_{Ex} = 433$ nm, $\lambda_{Em} = 628$ and 667 nm).[18] The excitation spectrum, monitored at both emission maxima, exhibits the same profile as the ground-state absorption spectra, showing the existence of a single emitting species.

Additionally, ATR-IR spectroscopy measurements were taken to confirm the presence of ZnP, as shown in Fig. S5.† Nonetheless, as the amount of incorporated ZnP is small compared to the TiO_2 matrix, ZnP signals are masked and could not be clearly distinguished.

The amount of ZnP incorporated in the films was estimated through UV-Vis absorption spectroscopy, as performed in our previous work.[23] ZnP content was estimated using the ellipsoidal pore dimensions ($a = 2$ nm, $b = c = 3.5$ nm), film thickness of ZnP@MTTF obtained from FE-SEM images ($t =$ 250 nm, Fig. S6†), absorbance of its Soret band and molar absorptivity of ZnP in solution ($\varepsilon^{436} = 1.81 \times 10^5$ M^{-1} cm^{-1}).[40] The obtained value is 14 μmol ZnP/g MTTF, equivalent to 7 molecules inside each pore (see ESI for details on calculations†). This value is in good agreement with the estimation obtained using the change in porosity from XRR measures, which gives 9 molecules per pore when comparing dry ZnP@MTTF and MTTF. If the sample is not previously dried, a larger value is obtained, due to increased water adsorption when the porphyrin is present (Fig. S1B†). Additionally, UV-Vis spectrum of the solution has been measured before and after film immersion (Fig. S7†), showing MTTF preconcentrates ZnP, removing nearly all of it from the solution. The resulting ZnP content is consistent with the values obtained for the adsorption of metalloporphyrins in MTTF-based photonic crystals and on the surface of TiO_2 nanoparticles.[23,41]

Dense, non-porous titania was also functionalized with ZnP as a control. Its UV-Vis absorption spectrum shows low incorporation of ZnP (Fig. S8†), meaning that the loading in ZnP@MTTF occurs within the pores. Moreover, if pore surface is not considered in the ZnP content estimation, assuming adsorption occurs outside the pores, a coverage of 6 molecules per nm^2 is obtained. This means porphyrin stacking would occur, since ZnP specific area is ~4 nm^2 per molecule, and agglomerates should be observed on the surface. Stacking would lead to the appearance of characteristic porphyrinic aggregation bands in the UV-Vis spectrum,[22,38,39] which is not the case for ZnP@MTTF.

ZnP@MTTF capability as a photocatalytic system was also investigated, since it has been shown that ZnP acts as a sensitizer in nanoparticle supported photocatalytic systems.[42] Reactions where electron transfer between a donor (ED) and an acceptor (EA) is photosensitized by MP, as shown in eqn (1) and (2), have been widely studied as a model for solar energy conversion and storage.[43]

$$EA + ED + MP \xrightarrow{h\nu} EA + ED + MP^* \quad (1)$$

$$EA + ED + MP^* \rightarrow EA^- + ED^+ + MP \quad (2)$$

Methylviologen (MV^{2+}, *N*,*N*′-dimethy-4,4′-bipyridinium cation) is one of the most studied EA.[44] MV^{2+} is reduced to its radical cation $MV^{\bullet+}$, which additionally can reduce other species, acting as an electron relay. This capability has been used in H_2 production with MP supported on nanoparticles, where MP in its excited state acts as the reducing agent and an ED later restores it to its oxidized form. Thus, in the presence of a catalyst such as Pt, $MV^{\bullet+}$ re-oxidizes to MV^{2+} generating H_2 (eqn (3)).[42]

$$2MV^{\bullet+} + 2H_2O \xrightarrow{Pt} 2MV^{2+} + 2H_2 + 2OH^- \quad (3)$$

Furthermore, $MV^{\bullet+}$ has a deep blue color, so the photoinduced reduction can be followed spectrophotometrically by measuring the $MV^{\bullet+}$ absorption band at 600 nm ($\varepsilon^{600} = 1.37 \times 10^4$ M^{-1} cm^{-1}).[45] Hence, reduction of MV^{2+} acts as a proof of concept for H_2 production. It is worth mentioning that poly(-viologens) in solution are able to diffuse through the MTTF porous structure,[46] enabling the use of MTTF pores as photocatalytic nanoreactors.

Following these guidelines, ZnP@MTTF was immersed in a MV^{2+} solution with triethanolamine (TEOA) as the ED. Upon irradiation using sun-like light the intense blue coloration of $MV^{\bullet+}$ appeared. Therefore, MV^{2+} molecules are capable of percolation to the porphyrin center inside the pores, where it is

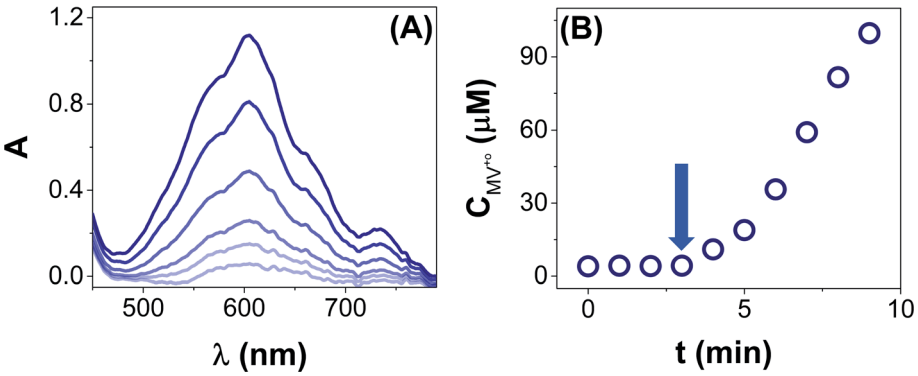

Fig. 3 UV-Vis absorption spectra of the reaction solution (A) and $MV^{\bullet+}$ concentration (B) at different irradiation times for ZnP@MTTF, the arrow indicates when irradiation is turned on.

reduced, and $MV^{\bullet+}$ diffuses back to the solution. Pictures of this experiment are shown in Fig. S9.† The concentration of $MV^{\bullet+}$ was determined every 1 minute by measuring the absorption spectra (Fig. 3A) and tracking the absorbance at 600 nm (Fig. 3B). Longer irradiation times were acquired, but absorbance was saturated. No $MV^{\bullet+}$ was observed in a control experiment with MTTF (Fig. S10†). Estimation of the initial rate for MV^{2+} reduction was calculated using the concentration of $MV^{\bullet+}$ generated in the first 6 minutes after irradiation is turned on. The obtained value of 809 μmol h^{-1} $\mu mol_{MP}{}^{-1}$ nearly duplicates the one observed in similar nanoparticle supported photocatalytic systems in suspension, which achieved a top value of 440 μmol h^{-1} $\mu mol_{MP}{}^{-1}$.[42] We believe that this proof of concept is promising for future applications in solar fuels or the solar-driven synthesis of organic molecules.[47]

MP have been widely used as photosensitizers, but their combination with MTTF needs further studies. Consequently, the possibility of dye sensitization in ZnP@MTTF was also tested. For these experiments, ZnP@MTTF was prepared on a transparent conductive FTO substrate and the setup depicted in Fig. S11† was used. Fig. 4A presents a chronoamperometry measured at 1.23 V (*vs.* RHE) with chopped illumination in the visible range, for both MTTF and ZnP@MTTF. A glass slide was used to filter UV light and account for the effect of ZnP as a sensitizer, observing a 47% increase in current when compared to bare MTTF. This behavior is observed at different potentials in a linear sweep voltammetry with chopped illumination (Fig. 4B). Negative potentials have also been explored (Fig. S13†). Overall current seems smaller than in other systems;[48] therefore, although ZnP@MTTF can be used for DSSC and DS-PEC devices, its more promising application is photocatalysis. It is worth noting that experiments were performed with no water oxidation catalyst included and with a low ZnP load. Further improvements can be made to increase light absorption and film crystallinity and conductivity, while still using 250 nm thick films, but are outside the scope of this work. Chronoamperometry was also performed without UV filtering (Fig. S12†), where MTTF absorption generates a larger photocurrent and the effect of sensitization can still be seen. Chronoamperometry at longer times showed a slight decrease in current (Fig. S14†), probably due to partial ZnP desorption caused by high electrolyte concentration interfering in electrostatic interactions with MTTF. Although these results are preliminary, they provide a sound basis for demonstrating that ZnP assists the photocatalytic performance of mesoporous titania thin films.

Conclusions

MP dyes like ZnP hold the potential to build efficient hybrid materials for energy harvest when combined with substrates like MTTF, which have unique structural properties and an organized pore network. The resulting hybrid material has physicochemical properties that derive from the substrate

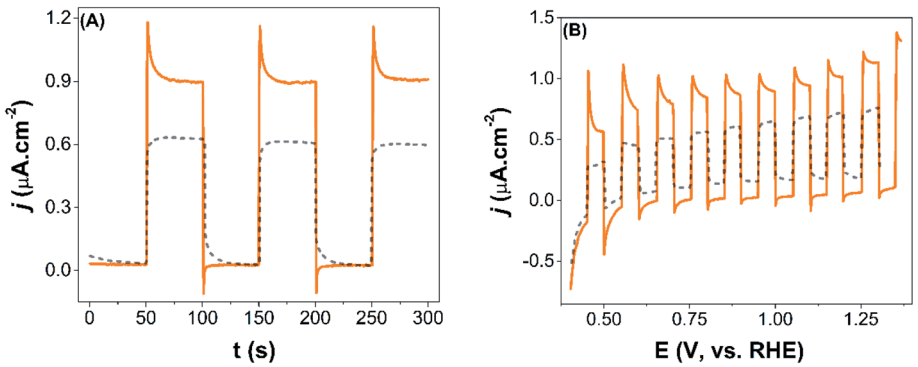

Fig. 4 Chronoamperometry at 1.23 V *vs.* RHE with chopped visible illumination for MTTF (black, dashed line) and ZnP@MTTF (orange, solid line) (A). Linear sweep voltammetry of MTTF (black, dashed line) and ZnP@MTTF (orange, solid line) with chopped visible illumination.

architecture, its optical transparency, ZnP molecular properties and new properties that arise from the combination. Furthermore, MTTF transparency makes photophysical measurements straightforward, and its high surface area incorporates large amounts of ZnP in an organized structure, allowing for better interaction with reagents. Furthermore, surface immobilization makes catalyst removal and replacement easier.

In this work, we successfully synthesized and characterized a new hybrid material, ZnP@MTTF. We have proved its photochemical activity through the evaluation of the MV^{2+} reduction assay, with results that almost double the activity of similar systems. ZnP@MTTF has the capability to produce a photocurrent, although it should be improved. More studies are underway in order to optimize the device's performance for its use in water splitting and other photocatalytic reactions. The nanostructured hybrid material we present here can be an alternative to the options that currently predominate, due to its simple and low-cost synthesis, which makes it suitable for large scale production.

Experimental

Materials and reagents

Zinc(II) 5,10,15,20-[*meso*-tetrakis(*N*-methylpyridyl) porphine] (ZnP) was purchased from Frontier Scientific. $TiCl_4$, non-ionic block-copolymer Pluronic F127 and absolute ethanol were obtained from Merck. Glass substrates were purchased from Biotraza. Fluorine doped tin oxide (FTO) substrates were purchased from Delta Technologies. Triethanolamine (TEOA) and other necessary reagents were acquired by Sigma-Aldrich. All chemicals were reagent grade and were used without further purification. Water was deionized and filtered using a Millipore water purification system (18 MΩ).

Mesoporous TiO_2 thin films

Mesoporous titania thin films (MTTF) were obtained onto different substrates according to literature procedures.[30,49] Initial sols were obtained by mixing $TiCl_4$, ethanol, copolymer template Pluronic F127 and water in a $1:40:5\times10^{-3}:10$ molar ratio. Films were deposited by dip-coating on clean substrates (glass or FTO) at 30 °C, 25–30% relative humidity and 3.0 mm s^{-1} withdrawal rate. As-prepared films were aged 24 h at 50% relative humidity. Further thermal treatment was performed by heating 24 h at 60 °C, 24 h at 130 °C and 2 h at 350 °C, with a heating ramp of 1 °C min^{-1}. This technique gives a crack-free MTTF, with a highly organized array of 8 nm diameter pore with an *Im*3*m* cubic structure.[50] Films with 30% pore volume and 250 nm thickness were used in this work. The pore size and the thickness of the films were obtained using Image-J software for analysis of the acquired SEM images.[51] Fig. S7† shows SEM images of the MTTF without modification.

Metalloporphyrin-mesoporous TiO_2 thin films (ZnP@MTTF)

The modification of the MTTF surface with ZnP was done by immersion for 48 h in a 30 μM solution of ZnP in water.[22] After adsorption, ZnP@MTTF was rinsed with deionized water and dried in a vacuum oven at 60 °C for 6 h.

Characterization

UV-Vis absorption spectra were recorded with an HP8453 diode array spectrophotometer in forward transmission mode using normal incidence geometry.

ATR-IR spectroscopy was performed on a Nicolet iN10 MX FTIR spectrometer in reflectance mode. All spectra were obtained as an average of 32 scans, at a 4.0 cm^{-1} resolution, in a range between 4000 and 650 cm^{-1}. Infrared data were processed using EZ-Omnic software.

Field Emission Scanning Electron Microscopy (FE-SEM) images were taken on an SEM Zeiss Supra 40 equipped with a field emission gun from CMA-FCEN-UBA.

X-ray reflectometry (XRR) measurements were performed with a Bruker D8 Eco equipment using an incident beam of Cu Kα radiation. To obtain accurate density values, measurements were performed under low-humidity conditions. This is a relevant experimental aspect, as the condensation of atmospheric moisture within the pores could lead to a severe underestimation of the film mesoporosity.

Steady-state emission was measured with an Edinburgh FS5 Spectrofluorometer, at 25 °C. Aqueous solutions were measured with air saturation, while films were measured in air using specially designed piece. Emission and excitation correction functions provided by the manufacturer were used.

Estimation of ZnP load in ZnP@MTTF

ZnP load was calculated as in Caraballo *et al.*[23] In order to estimate the amount of ZnP molecules adsorbed inside the mesopores we used the absorbance for ZnP@MTTF and the molar extinction of ZnP in solution. From the Lambert–Beer law, if the absorbance at 449 nm is due to ZnP and assuming that molar absorptivity does not change appreciably:

$$\mathrm{Abs} = \varepsilon^{436} \times [\mathrm{ZnP}] \times l_{\mathrm{MTTF}}$$

where $\varepsilon^{436} = 1.81\times10^{5}$ M^{-1} cm^{-1} and, determining MTTF width from SEM images, $l_{\mathrm{MTTF}} = 250\ \mathrm{nm} = 2.5\times10^{-5}$ cm.

Then, being 0.183 the absorbance at 449 nm for ZnP@MTTF, the obtained result of $[\mathrm{ZnP}] = 4.0\times10^{-2}$ mol dm^{-3} is equivalent to 2.4×10^{-2} molecules per nm^{-3} within the volume of the film. Knowing that the amount of $[\mathrm{ZnP}] = 2.4\times10^{-2}$ molecules per nm^{-3}, that these nanostructured films are ~34% porous when dried and that the pore volume is 103 nm^3, the number of ZnP molecules adsorbed within the ellipsoidal pores was determined to be 7 porphyrin molecules per pore. This result is an estimate, as not all the pores might have porphyrin inside, because its diffusion is limited by the tortuosity of the mesoporous material.

Photocatalytic assay

The methylviologen (MV^{2+}) reduction assay was performed following the procedure described by Tian *et al.*[42] ZnP@MTTF samples were immersed in a quartz cuvette in presence of MV^{2+}

(100 mM in degassed H_2O), TEOA (200 mM) as an electron donor and irradiated with a Xe lamp. The setup is depicted in Fig. S9.† The concentration of reduced MV^{2+} was measured by the change in absorbance at 600 nm near the peak of its radical anion band, every minute. No MV^{2+} reduction was observed in experiments performed with bare MTTF.

Photoelectrochemical assay

The photoelectrochemical measurements were conducted in a custom made photoelectrochemical cell, with a standard 3-electrode system (WE: ZnP@MTTF or MTTF, RE: Ag/AgCl (KCl 3 M), CE: Pt foil). The setup is depicted in Fig. S8.† A Metrohm Autolab potentiostat coupled with Nova software was used. Linear sweep voltammetries were carried out at 10 mV s^{-1} with chopped illumination. The light source was a 30 W Xe lamp, with a glass slide as UV-filter. Light was shone from the electrode-solution interface. Current densities are referred to the geometrical area of the samples. Potentials were converted to the reversible hydrogen electrode (RHE), according to eqn (4):

$$E(vs.\ \mathrm{RHE}) = E(vs.\ \mathrm{Ag/AgCl}) + 0.059 \times \mathrm{pH} \quad (4)$$

Author contributions

R. M. C.: investigation, formal analysis, visualization, writing – original draft (lead). P. V.: investigation, visualization, writing – original draft. F. H.: investigation, visualization, writing – original draft. G. S. I: conceptualization, funding acquisition, resources, writing – review. M. H.: conceptualization, funding acquisition, resources, supervision, writing – original draft (lead).

Conflicts of interest

There are no conflicts to declare.

Acknowledgements

This work was financially supported by Agencia I+D+i (PICT 2015-3526, 2016-0982, 2017-4651 and 2018-04236) and UNSAM. R. M. C. and P. V. thank CONICET for the fellowship grant. F. H. thanks Agencia I+D+i for his fellowship grant. G. J. A. A. S. I. and M. H. are members of CONICET.

References

1 G. P. Peters, R. M. Andrew, T. Boden, J. G. Canadell, P. Ciais, C. Le Quéré, G. Marland, M. R. Raupach and C. Wilson, *Nat. Clim. Change*, 2013, **3**, 4–6.
2 L. C. King and J. C. J. M. van den Bergh, *Nat. Energy*, 2018, **3**, 334–340.
3 X. Hu and K. Schulten, *Phys. Today*, 1997, **50**, 28–34.
4 R. Croce and H. Van Amerongen, *Nat. Chem. Biol.*, 2014, **10**, 492–501.
5 J. Otsuki, *J. Mater. Chem. A*, 2018, **6**, 6710–6753.
6 A. Antoniuk-Pablant, Y. Terazono, B. J. Brennan, B. D. Sherman, J. D. Megiatto, G. W. Brudvig, A. L. Moore, T. A. Moore and D. Gust, *J. Mater. Chem. A*, 2016, **4**, 2976–2985.
7 M. J. Griffith, K. Sunahara, P. Wagner, K. Wagner, G. G. Wallace, D. L. Officer, A. Furube, R. Katoh, S. Mori and A. J. Mozer, *Chem. Commun.*, 2012, **48**, 4145.
8 D. Sygkridou, A. Apostolopoulou, A. Charisiadis, V. Nikolaou, G. Charalambidis, A. G. Coutsolelos and E. Stathatos, *ChemistrySelect*, 2018, **3**, 2536–2541.
9 A. Mahmood, J. Y. Hu, B. Xiao, A. Tang, X. Wang and E. Zhou, *J. Mater. Chem. A*, 2018, **6**, 16769–16797.
10 A. B. Gallo, J. R. Simões-Moreira, H. K. M. Costa, M. M. Santos and E. Moutinho dos Santos, *Renewable Sustainable Energy Rev.*, 2016, **65**, 800–822.
11 F. Barbir, *Sol. Energy*, 2005, **78**, 661–669.
12 J. D. Holladay, J. Hu, D. L. King and Y. Wang, *Catal. Today*, 2009, **139**, 244–260.
13 P. Böhm and H. Gröger, *ChemCatChem*, 2015, **7**, 22–28.
14 Y. Liu, Y. Han, Z. Zhang, W. Zhang, W. Lai, Y. Wang and R. Cao, *Chem. Sci.*, 2019, **10**, 2613–2622.
15 C. Steinlechner and H. Junge, *Angew. Chem., Int. Ed.*, 2018, **57**, 44–45.
16 K. Ladomenou, M. Natali, E. Iengo, G. Charalampidis, F. Scandola and A. G. Coutsolelos, *Coord. Chem. Rev.*, 2015, **304–305**, 38–54.
17 Y. Wu, J. M. Veleta, D. Tang, A. D. Price, C. E. Botez and D. Villagrán, *Dalton Trans.*, 2018, **47**, 8801–8806.
18 K. Kalyanasundaram and M. Neumann-Spallart, *J. Phys. Chem.*, 1982, **86**, 5163–5169.
19 R. Kumar and M. Sankar, *Inorg. Chem.*, 2014, **53**, 12706–12719.
20 S. Ganapathy, G. T. Oostergetel, P. K. Wawrzyniak, M. Reus, A. Gomez Maqueo Chew, F. Buda, E. J. Boekema, D. A. Bryant, A. R. Holzwarth and H. J. M. de Groot, *Proc. Natl. Acad. Sci.*, 2009, **106**, 8525–8530.
21 Y. Chen, A. Li, Z.-H. Huang, L.-N. Wang and F. Kang, *Nanomaterials*, 2016, **6**, 51.
22 M. Hamer, R. M. Caraballo, P. J. Eaton and C. Medforth, *J. Porphyrins Phthalocyanines*, 2019, **23**, 526–533.
23 R. M. Caraballo, D. Onna, N. López Abdala, G. J. A. A. Soler Illia and M. Hamer, *Sens. Actuators, B*, 2020, **309**, 127712–127719.
24 S. Takagi, M. Eguchi, D. Tryk and H. Inoue, *J. Photochem. Photobiol., C*, 2006, **7**, 104–126.
25 A. A. Ismail and D. W. Bahnemann, *ChemSusChem*, 2010, **3**, 1057–1062.
26 X. Lü, W. Sun, J. Li, W. Xu and F. Zhang, *Spectrochim. Acta, Part A*, 2013, **111**, 161–168.
27 A. Yamamoto, Y. Mizuno, K. Teramura, S. Hosokawa, T. Shishido and T. Tanaka, *Catal. Sci. Technol.*, 2015, **5**, 556–561.
28 S. Mathew, A. Yella, P. Gao, R. Humphry-Baker, B. F. E. Curchod, N. Ashari-Astani, I. Tavernelli, U. Rothlisberger, M. K. Nazeeruddin and M. Grätzel, *Nat. Chem.*, 2014, **6**, 242–247.

29 M. H. Bartl, S. W. Boettcher, K. L. Frindell and G. D. Stucky, *Acc. Chem. Res.*, 2005, **38**, 263–271.
30 G. J. a. a. Soler-Illia, P. C. Angelomé, M. C. Fuertes, D. Grosso and C. Boissiere, *Nanoscale*, 2012, **4**, 2549.
31 I. L. Violi, M. D. Perez, M. C. Fuertes and G. J. A. A. Soler-Illia, *ACS Appl. Mater. Interfaces*, 2012, **4**, 4320–4330.
32 T. Higashino and H. Imahori, *Dalton Trans.*, 2015, **44**, 448–463.
33 E. L. Crepaldi, G. J. d. A. A. Soler-Illia, D. Grosso, F. Cagnol, F. Ribot and C. Sanchez, *J. Am. Chem. Soc.*, 2003, **125**, 9770–9786.
34 G. J. d. A. A. Soler-Illia, C. Sanchez, B. Lebeau, J. Patarin, B. P. Soler-Illia, G. J. A. A. Sanchez and C. Lebeau, *Chem. Rev.*, 2002, **102**, 4093–4138.
35 Q. Tang, P. C. Angelomé, G. J. A. A. Soler-Illia and M. Müller, *Phys. Chem. Chem. Phys.*, 2017, **19**, 28249–28262.
36 R. Gimenez, G. J. A. A. Soler-Illia, C. L. A. Berli and M. G. Bellino, *ACS Nano*, 2020, **14**, 2702–2708.
37 E. A. Malinka, G. L. Kamalov, S. V. Vodzinskii, V. I. Melnik and Z. I. Zhilina, *J. Photochem. Photobiol., A*, 1995, **90**, 153–158.
38 J. Roales, J. M. Pedrosa, M. G. Guillén, T. Lopes-Costa, S. M. A. Pinto, M. J. F. Calvete and M. M. Pereira, *Sens. Actuators, B*, 2015, **210**, 28–35.
39 M. Hamer and I. N. I. N. Rezzano, *Inorg. Chem.*, 2016, **55**, 8595–8602.
40 J. Mack and M. J. Stillman, in *The Porphyrin Handbook*, Elsevier, 2003, pp. 43–116.
41 D. Chen, D. Yang, J. Geng, J. Zhu and Z. Jiang, *Appl. Surf. Sci.*, 2008, **255**, 2879–2884.
42 Y. Tian, K. E. Martin, J. Y.-T. Shelnutt, L. Evans, T. Busani, J. E. Miller, C. J. Medforth and J. A. Shelnutt, *Chem. Commun.*, 2011, **47**, 6069.
43 D. Gust, T. A. Moore and A. L. Moore, *Acc. Chem. Res.*, 2009, **42**, 1890–1898.
44 M. Rougee, T. Ebbessen, F. Ghetti and R. V. Bensasson, *J. Phys. Chem.*, 1982, **86**, 4404–4412.
45 T. Watanabe and K. Honda, *J. Phys. Chem.*, 1982, **86**, 2617–2619.
46 S. Saint-André, F. Albanese, G. J. A. A. Soler-Illia and M. Tagliazucchi, *Phys. Chem. Chem. Phys.*, 2019, **21**, 2743–2754.
47 M. Sankar, Q. He, R. V. Engel, M. A. Sainna, A. J. Logsdail, A. Roldan, D. J. Willock, N. Agarwal, C. J. Kiely and G. J. Hutchings, *Chem. Rev.*, 2020, **120**, 3890–3938.
48 G. F. Moore, J. D. Blakemore, R. L. Milot, J. F. Hull, H. E. Song, L. Cai, C. A. Schmuttenmaer, R. H. Crabtree and G. W. Brudvig, *Energy Environ. Sci.*, 2011, **4**, 2389–2392.
49 C. S. G. J. A. A. Soler-Illia, E. L. Crepaldi and D. Grosso, *Curr. Opin. Colloid Interface Sci.*, 2003, **8**, 109–126.
50 E. D. Martínez, C. Boissière, D. Grosso, C. Sanchez, H. Troiani and G. J. A. A. Soler-Illia, *J. Phys. Chem. C*, 2014, **118**, 13137–13151.
51 A. Alvarez-Fernandez, B. Reid, M. J. Fornerod, A. Taylor, G. Divitini and S. Guldin, *ACS Appl. Mater. Interfaces*, 2020, **12**, 5195–5208.